

# ForceGrip: Data-Free Curriculum Learning for Realistic Grip Force Control in VR Hand Manipulation

DongHeun Han<sup>1</sup>  
hand32@khu.ac.kr

Byungmin Kim<sup>2</sup>  
kbmstar1@korea.ac.kr

RoUn Lee<sup>1</sup>  
dlfhdns@khu.ac.kr

KyeongMin Kim<sup>2</sup>  
kgm031189@gmail.com

Hyoseok Hwang<sup>1</sup>  
hyoseok@khu.ac.kr

HyeongYeop Kang<sup>2†</sup>  
siamiz\_hkang@korea.ac.kr

<sup>1</sup>Kyung Hee University, Yongin, South Korea

<sup>2</sup>Korea University, Seoul, South Korea

March 14, 2025

**Goal: Realistic hand manipulation in VR controller interfaces through faithful grip force control.**

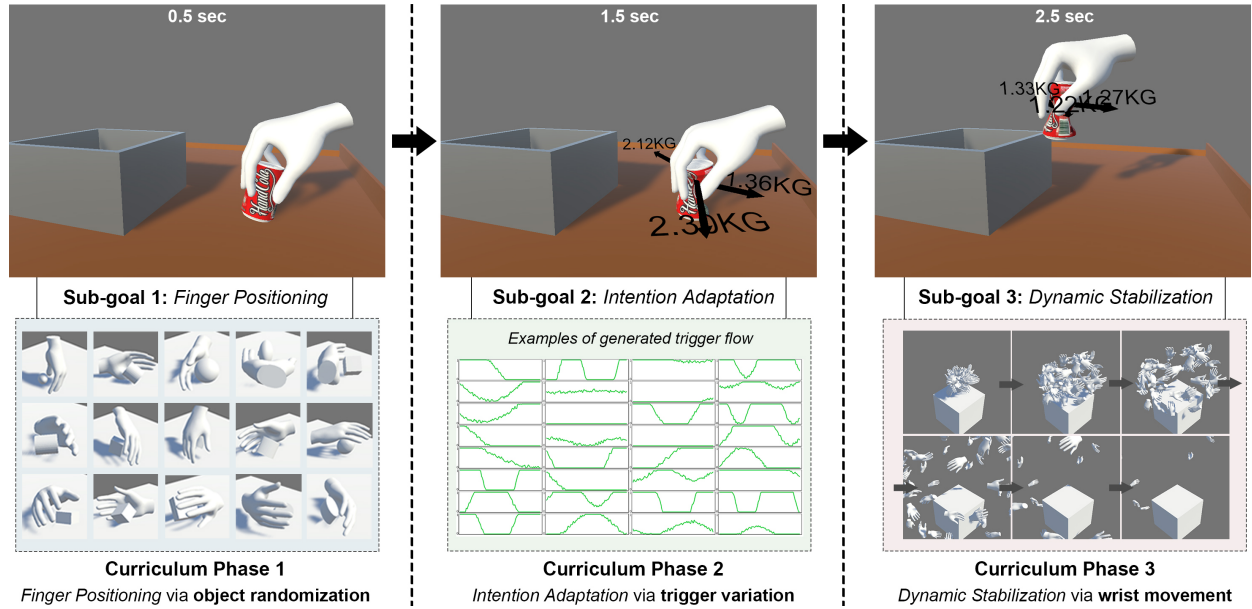


Figure 1: Overview of our training pipeline. Rather than relying on motion-capture data, we generate diverse scenarios of varying object shapes, user inputs, and wrist motions; a three-phase curriculum progressively increases task complexity.

## Abstract

Realistic Hand manipulation is a key component of immersive virtual reality (VR), yet existing methods often rely on a kinematic approach or motion-capture datasets that omit crucial physical attributes such as contact forces and finger torques. Consequently, these approaches prioritize tight, one-size-fits-all grips rather than reflecting users' intended force levels. We present *ForceGrip*, a deep learning agent that synthesizes realistic hand manipulation motions, faithfully reflecting the user's grip force intention. Instead of mimicking predefined motion datasets, ForceGrip uses generated training scenarios-randomizing object shapes, wrist movements, and trigger input flows—to challenge the agent with a broad spectrum of physical interactions. To effectively learn from these complex tasks, we employ a three-phase curriculum learning framework comprising *Finger Positioning*, *Intention Adaptation*, and *Dynamic Stabilization*. This progressive strategy ensures stable hand-object contact, adaptive force control based on user inputs, and robust handling under dynamic conditions. Additionally, a proximity reward function enhances natural finger motions and accelerates training convergence. Quantitative and qualitative evaluations reveal ForceGrip's superior force controllability and plausibility compared to state-of-the-art methods. The video presentation of our paper is accessible at <https://youtu.be/1R-YAfninJw>.

**Keywords:** Virtual reality, Hand manipulation, Interaction, Physics-based animation, Curriculum learning

# 1 Introduction

Immersive hand interaction is vital for compelling virtual reality (VR) experiences, enabling users to naturally grasp and manipulate objects. Although controller-based interfaces have become prevalent due to their accessibility, usability and responsiveness Han et al. [2023], most existing solutions overlook the nuanced control of grip force, focusing instead on reproducing visually plausible hand motions. This gap undermines a key dimension of realistic interaction: in physical environments, users continually fine-tune their grip force to accommodate differences in object weight, fragility, and friction, allowing objects to slip under varying force levels or remain firmly secured when needed.

Translating these nuances into VR poses considerable challenges, as conventional datasets and motion-capture techniques rarely include detailed physical attributes such as contact forces or finger torques. Consequently, it is crucial to provide diverse scenarios that involve various physical demands and ensure that these complex scenarios can be effectively learned.

To address this gap, we introduce *ForceGrip*, a deep learning agent that translates VR controller inputs into realistic grip force dynamics. Rather than imitating static motion captures, ForceGrip learns from randomly generated scenarios that vary object shape, trigger signals, wrist movements and external conditions. Our curriculum learning framework systematically increases complexity through three phases: *Finger Positioning*, *Intention Adaptation*, and *Dynamic Stabilization*. We further incorporate a proximity-based reward to guide natural fingertip contact, accelerating training and foster natural finger movements without imitating reference motion data.

In summary, our key contributions are as follows:

- I. **Dataset-free training.** ForceGrip synthesizes visually and physically realistic hand manipulations without relying on motion-capture data.
- II. **User-controlled grip force.** By faithfully translating users’ grip force intentions into realistic hand motions, ForceGrip significantly improves interaction precision and immersion.
- III. **Effective curriculum learning.** We demonstrate how incremental training phases handle diverse, high-complexity VR hand interactions with robust convergence.

## 2 Related Works

### 2.1 VR Interfaces for Physical Interaction Modeling

Two principal approaches exist for hand interactions in VR: **hand-tracking** and **VR controller** interfaces. Hand-tracking interfaces rely on sensors, such as VR gloves or vision-based sensors, offering high embodiment by mirroring the user’s actual hand movements Voigt-Antons et al. [2020]. However, they often use penetration-based models for grip force Höll et al. [2018], Quan et al. [2020], which require careful per-finger calibration and can undermine usability and confidence Voigt-Antons et al. [2020], Kangas et al. [2022]. Furthermore, task performance depends on the sensing hardware quality Viola et al. [2022], restricting the general user’s accessibility.

In contrast, VR controller interfaces treat the controller’s pose as the wrist proxy, while finger motions are either explicitly generated or inferred. A basic technique is the attachment-based method Oprea et al. [2019], Shi et al. [2022], which triggers fixed finger-closing motions and attaches objects upon collision. Although intuitive to use, it lacks motion diversity and physical realism. VR-HandNet Han et al. [2023] addresses some of these issues by inferring joint torques from virtual sensor data and comparing them to motion-capture datasets. However, because these datasets often lack physical parameters—such as contact forces and finger torques—the system’s ability to provide fine-grained grip force control remains constrained.

Table 1 summarizes existing methods. Building on these insights, our study proposes a controller-based, physics-based, and learning-based approach that does not rely on reference motion data.

### 2.2 Physics-based Animation Training

Physics-based animation calculates joint torques via a physics engine to account for collisions, balance, and other constraints, enabling systems to adapt dynamically to environmental changes and external forces. Popular engines Todorov et al. [2012], Coumans and Bai [2016], Liang et al. [2018], Makovychuk et al. [2021] often lack differentiability or smooth integration with deep learning. Although differentiable engines exist Hu et al. [2019], Freeman et al. [2021], they see limited use due to computational overhead and restricted physics features. Consequently, reinforcement learning (RL) Sutton and Barto [1999] serves as the dominant method, as it trains agents via reward signals without requiring differentiability.

Table 1: Structured comparison of existing VR hand manipulation methods by presenting whether they are controller-based, involve physics simulation, employ learning-based strategies, or require a reference motion dataset.

	Controller based	Physics based	Learning based	Reference Data Free
Penetration				
Höll et al. [2018]	X	O	X	O
Quan et al. [2020]				
Attachment				
Oprea et al. [2019]	O	X	X	O
VR-HandNet				
Han et al. [2023]	O	O	O	X
<b>ForceGrip</b>	O	O	O	O

In general, physics-based animation research addresses three key goals: animation reproduction, task completion, and user control.

In animation reproduction research, the objective is to replicate target motions within a physically simulated environment for enhanced realism. Techniques such as imitation reward Peng et al. [2017, 2018], Park et al. [2019], Won and Lee [2019], Lee et al. [2021b] and generative adversarial imitation learning (GAIL) Ho and Ermon [2016] are often adopted to align simulated poses with reference motion data Luo et al. [2020], Peng et al. [2021, 2022], Hassan et al. [2023]. This approach preserves natural motion quality but can be limited by the coverage of available datasets.

In task completion research, agents learn specific tasks such as locomotion Heess et al. [2017], Klipfel et al. [2023], object manipulation Kumar and Todorov [2015], Andrychowicz et al. [2020], Christen et al. [2022], Zhang et al. [2024], or specialized actions like door opening Rajeswaran et al. [2017] or chopstick handling Yang et al. [2022].

In user control research, real-time user inputs dynamically reshape the agent’s objectives, integrating animation reproduction for smooth, natural responses. Examples include determining walking directions Bergamin et al. [2019], Wang et al. [2020], Won et al. [2022], generating diverse skill animations Lee et al. [2021a], and controlling animations through natural language Juravsky et al. [2022], Cui et al. [2024]. For hand-specific control, VR controllers can provide user signals used for finger motion simulation Han et al. [2023].

Building on these foundations, our research focuses on user control with an emphasis on precise grip force translation.

### 2.3 Curriculum Learning

Curriculum learning Bengio et al. [2009] organizes training tasks in increasing order of difficulty, a strategy shown to accelerate convergence and improve performance in deep learning Weinshall et al. [2018], Baker et al. [2019], Hacoheh and Weinshall [2019].

Within physics-based animation, this approach helps agents learn complex skills more efficiently. For example, Won et al. [2021] first trained basic skills and then introducing adversarial environments. Similarly, Liu et al. [2022], Luo et al. [2023], Haarnoja et al. [2024] guides agents to learn increasingly diverse and challenging skills. Although automated task sequence generation has been explored Graves et al. [2017], Florensa et al. [2018], Silva and Costa [2018], Narvekar and Stone [2018], no universal standard exists for defining task difficulty Narvekar et al. [2020]. Instead, manual structuring remains highly effective Justesen et al. [2018], Cobbe et al. [2019], Wang et al. [2019].

In this work, we devise a structured curriculum to address the challenges of grip force control in VR.

## 3 Overview

Figure 1 depicts our training pipeline. We employ Unity with NVIDIA PhysX for real-time physics, updating at 120 Hz while the learning agent acts at 30 Hz. Each time step  $t$ , the agent outputs torques for finger joints, which a proportional-derivative (PD) controller Tan et al. [2011] translates into hand poses and drives object interactions at time  $t + 1$ . During training, the wrist follows pre-set motion paths, whereas in actual usage it follows VR controller movements.

Instead of relying on motion-capture data, we generate diverse scenarios encompassing varied object shapes, user inputs, and wrist motions to prevent overfitting and enhance realism. However, this variability

increases learning complexity. To address this, our curriculum strategy partitions training into simpler grip tasks, followed by progressively more dynamic conditions.

To train the agent, we leverage RL. We use proximal policy optimization (PPO) Schulman et al. [2017], running 576 concurrent agents with different seeds to maximize training diversity. Detailed hyperparameter settings are given in the supplementary materials. Additionally, we employ *early termination* Peng et al. [2018] to stop an episode if an object moves more than 10 cm away from the wrist, avoiding wasted computation on irrecoverable states. This mechanism increases efficiency and prevents spurious rewards, ultimately leading to a more stable policy that can handle the intricate demands of VR grip force control.

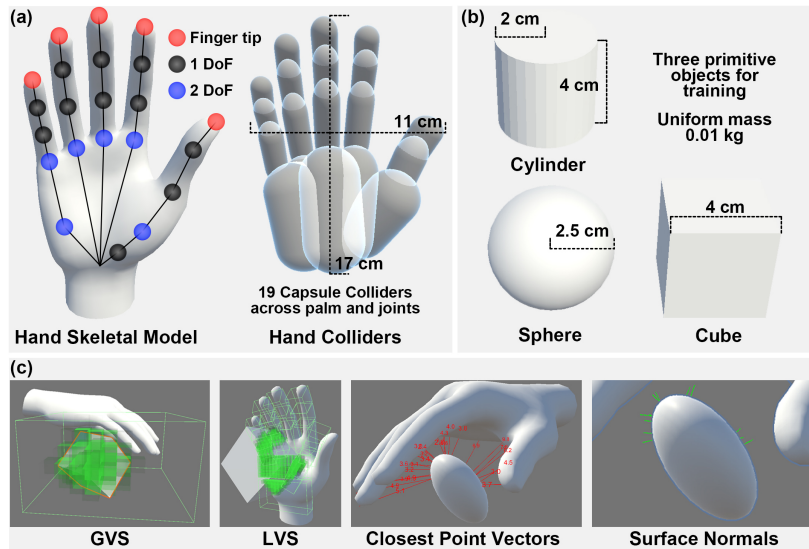


Figure 2: (a) Hand model from Meta XR Core SDK. (b) Objects: sphere, cube, and cylinder. (c) Sensors: GVS, LVS, closest and normal vector.

### 3.1 Hand Model and Objects

We utilize the Meta XR Core SDK hand model, which has 17 finger joints (23 total DoFs) and 19 capsule colliders spread across the fingers and palm (Figure 2(a)). To learn various grip conditions, we use three primitive object shapes—sphere, cube, and cylinder (Figure 2(b))—each with a uniform mass of 0.01 kg. Rather than ensuring all objects can always be lifted, our objective is to reflect user-intended force; insufficient force causes objects to slip. However, since dropping an object triggers early termination and thus biases the agent to apply overly strong grips, we mitigate mass effects by keeping these objects lightweight.

### 3.2 State and Action

ForceGrip is a deep RL agent that receives an environment state  $s \in \mathbb{R}^{3023}$  and outputs an action  $a \in \mathbb{R}^{23}$  at each time step. The state  $s$  comprises three primary components: hand model information ( $H$ ), object information ( $O$ ), and task information ( $T$ ).

Hand model information  $H = \{p, q, v, w, \alpha\}$  includes joint positions  $p \in \mathbb{R}^{66}$ , joint DoF angles  $q \in \mathbb{R}^{23}$ , joint linear velocities  $v \in \mathbb{R}^{51}$ , joint DoF velocities  $w \in \mathbb{R}^{23}$ , and joint DoF accelerations  $\alpha \in \mathbb{R}^{23}$ . All positional attributes are expressed in meters and shifted into a wrist-centric coordinate system, while angular values use radians to standardize feature ranges.

Object information  $O = \{o_g, v_{gvs}, v_{lvs}, c, n\}$  includes the gravity vector  $o_g \in \mathbb{R}^3$  in wrist coordinates, a global voxel sensor  $v_{gvs} \in \mathbb{R}^{450}$  attached to the wrist, employing 2 cm cells, local voxel sensors  $v_{lvs} \in \mathbb{R}^{2160}$  attached to each collider, employing 0.5 cm cells, closest point vectors  $c \in \mathbb{R}^{69}$  from relevant joints to the object’s surface, and corresponding surface normals  $n \in \mathbb{R}^{69}$ . Inspired by previous work Zhang et al. [2021], Han et al. [2023], this dual-resolution sensing strategy provides a balance between detail and generality, minimizing overfitting to a specific object shape. Object information is illustrated in Figure 2.

Task-related information  $T = \{f, u, p\}$  comprises current force vectors for each collider  $f \in \mathbb{R}^{57}$ , user trigger signal history  $u \in \mathbb{R}^6$  over the past 6 frames (0.2 s), and previous action  $p \in \mathbb{R}^{23}$ . By incorporating past user inputs and recent actions, the agent can regulate grip forces more smoothly and maintain consistent hand-object contact.

### 3.3 Reward function

The agent’s primary goal is to translate user trigger signals into physically plausible grip forces. We define a *force reward*  $r_f$  as follows:

$$r_f = \exp[-1.0(\|\sum_k f_t^k\| - f_t^{target})^2] \quad (1)$$

where  $f_t^k$  represents the per-collider force vectors at time  $t$ , and  $f_t^{target}$  is the target grip force derived from the user’s input by

$$f_t^{target} = f_{max} \cdot \bar{u}_t \quad (2)$$

Here,  $f_{max} = 10$  kgf is the maximum grip force, and  $\bar{u}_t$  is the average trigger signal over recent six frames. Note that the value of  $f_{max}$  can be adjusted for different applications to accommodate varying device or interaction requirements.

Relying solely on a task-centric reward can yield stiff, unnatural hand motions, so we introduce a *proximity reward*  $r_p$  to guide initial contact:

$$r_p = \sum_j w^j \exp[-0.07\|c_t^j\|^2] \quad (3)$$

where  $c_t^j$  is the distance vector from the  $j$ -th joint to the object surface, and  $w^j$  is a weight emphasizing fingertip-first contact. We assign higher weights (0.0625) to the five end-effectors and their associated joints, and lower weights (0.03125) elsewhere.

The final reward combines these two terms:

$$r = r_f + r_p \quad (4)$$

### 3.4 Model Architecture

At each timestep, the agent processes the state  $s$  by splitting it into logically distinct components:  $p, q, v, w, \alpha, o_g, v_{gvs}, v_{lvs}, c, n, f, u, p$ , embedding each subset with specialized encoder layers and concatenating the results into a 580-dimensional vector. This vector then passes through 10 fully connected layers (580 neurons each, GeLU Hendrycks and Gimpel [2016], producing 23 action values that control joint torques. Additional architectural details, including encoder configurations and hyperparameters, appear in the supplementary materials.

## 4 Training

### 4.1 Training scenario generation

To ensure broad adaptability and avoid limited-coverage datasets, we generate 3-second (90-frame) training scenarios rather than relying on motion-capture data. Although many VR tasks lack a strict endpoint, we treat these scenarios as repeating episodes in real-world deployment.

Our training scenarios incorporate three key factors:

**Object randomization** Each episode randomly scales objects along  $x, y$ , and  $z$ -axis by factors between 0.5 and 1.5 and arbitrarily positions them within a predefined volume in front of the hand. During the first 0.5 seconds, object stabilization is performed. Each object is rendered kinematic (i.e., not influenced by physics) to stabilize poses, allowing the agent’s fingers to approach the object without premature slipping.

**Trigger Variation.** We synthesize noisy trigger signals by combining sinusoidal functions with Gaussian noise. Varying frequencies, amplitudes, and offsets prevents overfitting to any single control pattern. Supplementary materials detail the parameters and sample waveforms.

**Wrist movement** After object stabilization, we remove the floor and introduce randomized wrist (up to  $2 m/s^2$ ) and angular (up to  $360^\circ/s^2$ ) accelerations at each physics simulation step. This reflects the dynamic real-world conditions and challenges the agent to maintain stable grip forces.

## 4.2 Curriculum learning

Because these random, high-complexity scenarios pose significant training challenges, we devise a three-phase curriculum: *Finger Positioning*, *Intention Adaptation*, and *Dynamic Stabilization*. Each phase builds on the skills developed in the preceding phase, progressively training the agent to handle increasingly dynamic and realistic conditions.

### 4.2.1 Phase 1: Finger Positioning

This phase trains the agent to establish accurate finger contact. To minimize distractions, only **object randomization** is active; *trigger variation* and *wrist movement* are disabled. The wrist remains fixed, and user triggers are set to constant random values within  $[0,1]$ . This setup accelerates the agent’s mastery of foundational behaviors such as collision handling and initial grip formation.

### 4.2.2 Phase 2: Intention Adaptation

Building on Phase 1, we add **trigger variation**, requiring the agent to interpret fluctuating signals and apply proportionate forces in real time.

### 4.2.3 Phase 3: Dynamic Stabilization

Building on Phase 2, we add **wrist movement**, introducing abrupt orientation and acceleration changes. Successful policies must preserve contact forces without losing grip, even when gravity and inertial forces vary substantially.

In our experiments, phase 1 trained for 1200 epochs, followed by 400 epochs of Phase 2, and then Phase 3 until reward convergence (800 epoches empirically).

## 5 Curriculum and Ablation Study

We evaluated our curriculum learning strategy and conducted ablation studies to assess the impact of specific design choices.

### 5.1 Test Conditions

Recall that our curriculum comprises three sequential phases: *Finger Positioning* (P1), *Intention Adaptation* (P2), and *Dynamic Stabilization* (P3). This aims to decompose randomized factors—such as varying trigger inputs and wrist motions—into progressively challenging phases, thereby improving learning stability in physically simulated VR environments.

To analyze alternative curriculum design, we introduce two additional phase variants: *Intention Adaptation* but with wrist movement instead of trigger variation (P2-b) and *Dynamic Stabilization* but with trigger variation instead of wrist movement (P3-b).

Based on these phases (P1, P2, P2-b, P3, P3-b), we define six distinct curricula:

- *C1 (Baseline)*:  $P1 \rightarrow P2 \rightarrow P3$ .
- *C2 (Swapper Factor)*:  $P1 \rightarrow P2\text{-b} \rightarrow P3\text{-b}$ .
- *C3 (Merged P2 and P3)*:  $P1 \rightarrow P2+P3$ .
- *C4 (Merged P1 and P2)*:  $P1+P2 \rightarrow P3$ .
- *C5 (Merged P1 and P2 for C2)*:  $P1+P2\text{-b} \rightarrow P3\text{-b}$ .
- *C6 (No Curriculum)*:  $P1+P2+P3$ .

Here, “merged” phases indicate that two sets of randomization factors (e.g., trigger variation and wrist movement) are introduced simultaneously rather than sequentially.

In addition to examining the curriculum, we conduct two additional ablation experiments to investigate the impact of design choices:

- *PR* ×: Remove the *proximity reward*, originally included to encourage lifelike fingertip contact and natural hand poses.

- $EL \times$ : Remove the *encoder layers* responsible for extracting domain-relevant information from each feature subset.

Both ablation conditions use the C1 curriculum with the same epoch-based transitions to ensure fair comparisons. In preliminary analyses, we confirmed that these phase-transition epochs did not adversely affect convergence when applied consistently across all setups. Note that, for  $EL \times$ , voxel-based encoders for  $v_{gvs}$  and  $v_{lvs}$  were retained to ensure the model’s trainability, given the large feature sizes of these components.

## 5.2 Evaluation Results

To investigate the training progression, we measured reward in every epoch for each curriculum and ablation setting. Figure 3 illustrates reward curves presenting how the agent’s performance evolves over time. Curricula that do not begin with P1 ( $C4$ ,  $C5$ , and  $C6$ ) exhibit noticeably lower rewards throughout training. This outcome emphasizes learning stable finger contact before introducing additional complexities, such as random wrist movement or realistic trigger inputs. Among the curricula, our proposed approach ( $C1$ ) achieves the highest overall reward.

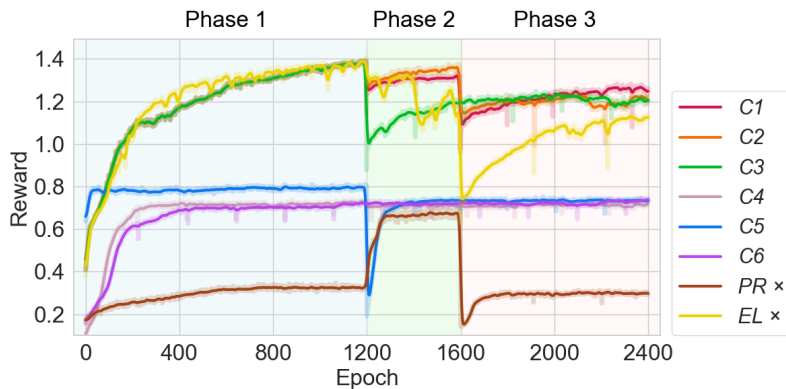


Figure 3: Reward curves for the different curriculum designs ( $C1$ – $C6$ ) and ablation experiments ( $PR \times$ ,  $EL \times$ ). The vertical lines at epochs 1200 and 1600 mark the transitions between Phases 1, 2, and 3. Note that in the  $PR \times$  condition, the reward values are doubled because only a single reward term remains once the proximity reward is removed.

For a more in-depth analysis, we collected data from 100,000 episodes and measured three key metrics: episode success ratio (ESR), average proximity reward (PR), and average force reward (FR). Table 2 presents the quantitative results. While  $C4$ ,  $C5$ , and  $C6$  maintain relatively acceptable ESR and PR scores, their lower FR scores reveal difficulties in managing force control when advanced randomization (e.g., full wrist movement or dynamic triggers) is introduced early. By contrast,  $C2$  and  $C3$ —which incorporate key phases in a more structured sequence—yield moderate ESR but fall below  $C1$  in overall stability. Removing the proximity reward ( $PR \times$ ) significantly reduces performance, particularly in ESR and PR, but also affects FR. Although eliminating encoder layers ( $EL \times$ ) achieves a higher ESR and PR, it simultaneously lowers the FR score. This outcome suggests that the network, lacking encoder-based feature extraction, struggles to incorporate critical low-dimensional inputs (e.g.,  $u \in \mathbb{R}^6$ ), causing the agent to adopt an overly forceful grip rather than refining grip force precision.

Table 2: Quantitative evaluation results. The highest score in each row is **bold and underlined**, and the second-highest is underlined only.

	$C1$	$C2$	$C3$	$C4$	$C5$	$C6$	$PR \times$	$EL \times$
ESR (%)	<b><u>81.30</u></b>	73.96	74.33	75.33	77.06	79.38	43.26	<b><u>83.44</u></b>
PR	<u>0.635</u>	0.601	0.595	0.589	0.605	0.607	0.014	<b><u>0.657</u></b>
FR	<b><u>0.607</u></b>	0.594	<u>0.601</u>	0.123	0.120	0.126	0.133	0.460

Overall, these findings confirm that a carefully structured curriculum—initiating with stable finger contact, followed by progressive introduction of force variation and wrist movement—affords both higher success rates and more realistic grip forces. Furthermore, ablation results emphasize the importance of our design choices, such as the proximity reward and encoder layers, in achieving robust and precise grip force control.

## 6 User Study

User experience is crucial when assessing the effectiveness of VR interaction techniques, especially those involving detailed hand manipulation. To present the superiority of our method, *ForceGrip* (FG), we conducted a comparative user study against two state-of-the-art VR controller interface methods: *Attachment* (AT) Oprea et al. [2019] and *VR-HandNet* (VH) Han et al. [2023].

### 6.1 Evaluation Metrics

To evaluate visual realism, we adopted the Realism Questionnaire (RQ) proposed by Oprea et al. [2019] containing 14 items across three categories: motor control, finger movement realism, and interaction realism. The individual scores are then aggregated into category-specific and overall indices, providing insights into perceptual realism from a purely visual standpoint.

To evaluate physical user experience, we devised a *Force Realism Questionnaire* (FRQ). Inspired by Gonzalez-Franco and Peck [2018] and tailored to physically simulated hand interactions, the FRQ retains the RQ’s three-category framework but focuses on evaluating *grip force* accuracy and user intention. Detailed FRQ items and scoring procedures are provided in the supplementary material.

To ensure that user comfort did not skew any evaluations, we employed the Simulator Sickness Questionnaire (SSQ) Kennedy et al. [1993] at the beginning and conclusion of each condition.

We applied the Friedman test to detect statistically significant differences, as the data did not meet the normality assumptions required by parametric tests. For post-hoc analysis, we conducted Wilcoxon signed-rank tests.

### 6.2 Participants and Apparatus

We recruited 20 participants (13 males and 7 females;  $\mu = 23.1, \sigma = 1.55$ ), comprising 11 individuals with prior VR experience and 9 newcomers. Each participant practiced all three interface methods (FG, VH, AT) for 5 minutes each, with additional practice time available upon request to ensure comfort with the controls.

We conducted the experiment using an Oculus Quest 2 headset and a stock controller, powered by a desktop featuring an NVIDIA RTX 3080 GPU and an AMD Ryzen 5 5600G CPU. This setup provided consistent performance across all trials, minimizing hardware-induced variability.

### 6.3 E1: Pick-and-place — Method

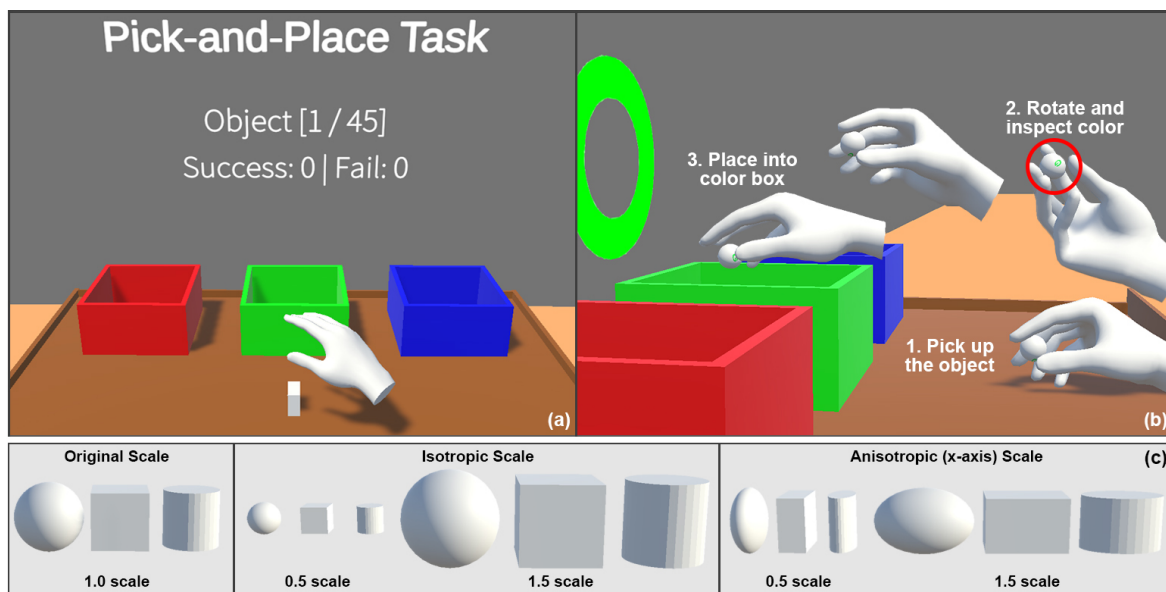


Figure 4: **Pick-and-place task.** (a) Randomly generated objects with color label pairs (R, G, or B). (b) Procedure: pick up the object, rotate and inspect its color label, and place it into the corresponding color box. (c) 15 candidate objects are displayed at three scales: original, isotropic, and anisotropic.



To evaluate visual realism in common object-handling scenarios, such as grasping, rotating, and translating, we designed a *Pick-and-Place* task (Figure 4).

Each participant completed three blocks in random order, with each block dedicated to one of three methods: FG, VH, and AT. Within each block, participants encountered 15 distinct objects—three at their original scale, six isotropically scaled along either  $x$ -,  $y$ -, or  $z$ -axis (by 0.5 and 1.5), and six anisotropically scaled along the  $x$ -axis (also by 0.5 and 1.5). Each object was assigned one of three color labels (R, G, or B), resulting in 45 unique object-label pairs per block.

With these 45 object-label pairs, participants were asked to perform *Pick-and-Place* task. Whenever a random object appeared in front of them, participants were instructed to pick it up, inspect the color label (R, G, or B) on its underside, and place it into the corresponding colored box. These 45 pairs were presented in a randomized order, ensuring no repeated pairings within the same block. Consequently, each participant completed a total of 135 *Pick-and-Place* (3 blocks  $\times$  45 pairs per block). Each block took approximately five minutes, followed by a two-minute break to mitigate fatigue. At the end of each block, participants completed RQ.

## 6.4 E1: Pick-and-Place — Results

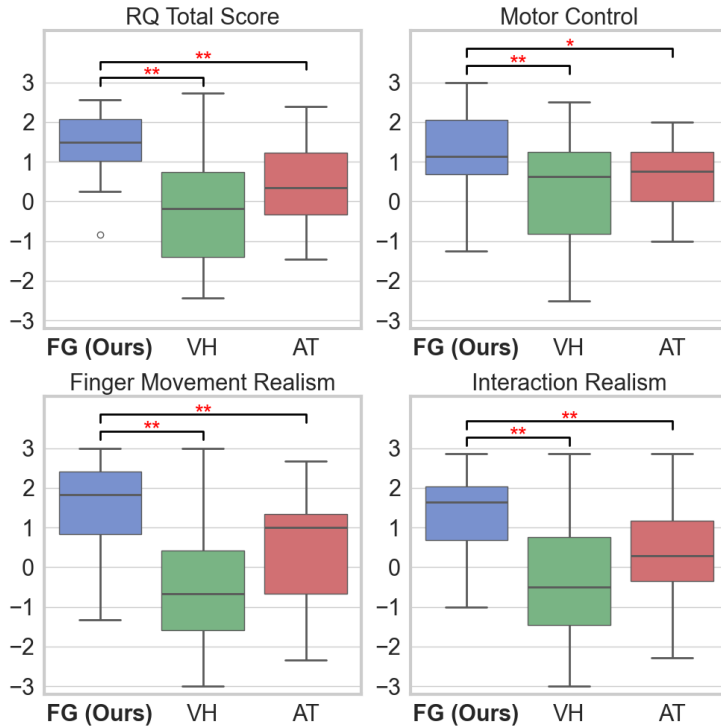


Figure 5: RQ scores for the Pick-and-Place task, using a 7-point Likert scale ranging from -3 (strongly disagree) to +3 (strongly agree). Brackets indicate statistical significances ( $*$  :  $p < .05$ ,  $**$  :  $p < .01$ ).

In terms of RQ scores, a Friedman test revealed significant differences across all interfaces ( $p < .01$ ). As shown in Figure 5, post-hoc Wilcoxon signed-rank tests confirmed that FG achieved significantly higher RQ scores than both VH and AT. Detailed statistical comparisons are provided in the supplementary materials. Additionally, there was no significant change in SSQ scores before and after the experiment, indicating minimal motion-sickness effects.

Participants provided qualitative observations that illuminated each technique’s strengths and limitations. For FG, participants praised its ability to “*stably and realistically grasp small objects*” (P3, P7, P12) and “*naturally adapt finger motions to varied shapes*” (P6, P9, P11, P13, P14, P19, P20). Some, however, experienced occasional “*object slipping*” (P3, P6, P10), likely arising from the rigid-body collision implementation of the capsule colliders at the fingertips.

For VH, participants praised its ability to “*natural dropping of objects, much like real life*” (P4, P8), highlighting the advantages of physics-based animation. Yet, many participants criticized its “*unnatural and predefined finger-closing motion*” (P1, P2, P4, P6, P8, P12, P13, P16, P19) and “*difficulty handling smaller objects*” (P3, P7, P10, P12, P14, P18), suggesting limited adaptability—a consequence of its narrower

motion-capture dataset coverage.

For AT, Participants observed “*naturally aligned finger posture for larger objects*” (P4, P6, P7, P12, P16, P18), but found “*grasping small items challenging*” (P4, P6, P7, P11, P12, P13, P16, P18). Others noted that “*unnatural and inconvenient experience stem from actions only triggered after palm sensor activation*” (P1, P3, P8, P10, P13, P18). These reflect AT’s inability to adapt various object shapes due to the inherent limitation of the kinematic approach.

Overall, this experiment indicates that *ForceGrip* provides superior visual realism for typical object manipulation tasks.

## 6.5 E2: Can squeeze — Method

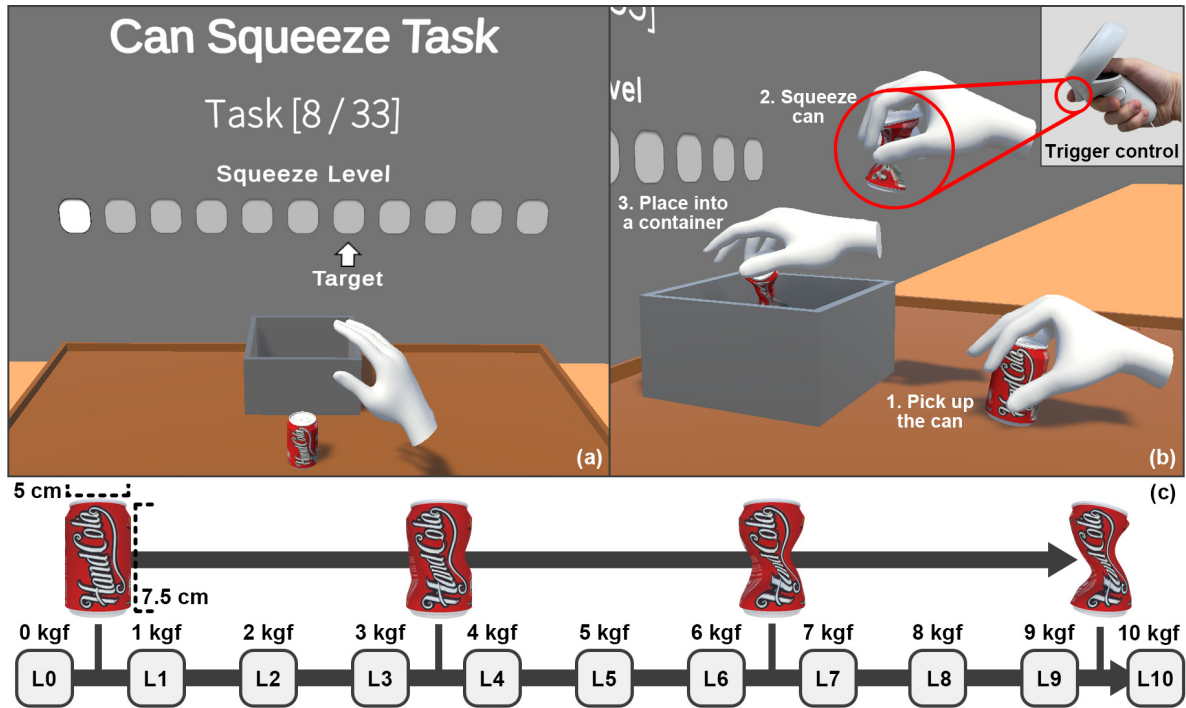


Figure 6: **Can squeeze task.** (a) Generated can object with a random target level. (b) Procedure: pick up the can, squeeze it via trigger control, and place it into the container. (c) Can deformation levels (L0: no deformation - L10: maximum deformation) visualized with mesh representations.

To evaluate how precisely users can translate controller-trigger inputs into physically simulated grip forces, we introduced the *Can Squeeze* task (Figure 6). Because AT does not support physical interactions, it was excluded from this experiment.

Participants were presented with a virtual can-shaped object modeled after standard beverage cans. They were then asked to deform it to a target level ranging from 0 (no deformation) to 10 (maximum deformation). Each integer increment (from 0-10) corresponded to a 1 kgf increase in force. We adopted this discrete, 11-level scale to balance force granularity with the limited sensitivity of typical VR controller triggers. In preliminary testing, subdividing the force range more finely led to confusion and reduced accuracy, as participants struggled to modulate shallow trigger inputs with greater precision.

At the start of each trial, a can was introduced in front of the user while a random target deformation level appeared on the display. The participant then adjusted the VR controller’s trigger to deform the can until it closely matched the target level, and subsequently placed the deformed can into a designated container. During the interaction, both visual and auditory feedback—implemented through mesh updates and sound effects—indicated the extent of can deformation.

Each participant completed two blocks, with one block dedicated to the FG and the other to VH. The order of these blocks was counterbalanced across participants. Within each block, 33 trials were conducted by repeating every target deformation level (0–10) three times, in randomized order. Consequently, each participant performed a total of 66 trials (2 blocks × 33 trials per block). Each block took approximately five minutes to complete, followed by a two-minute break to mitigate fatigue. At the end of each block, participants completed FRQ.

## 6.6 E2: Can squeeze — Results

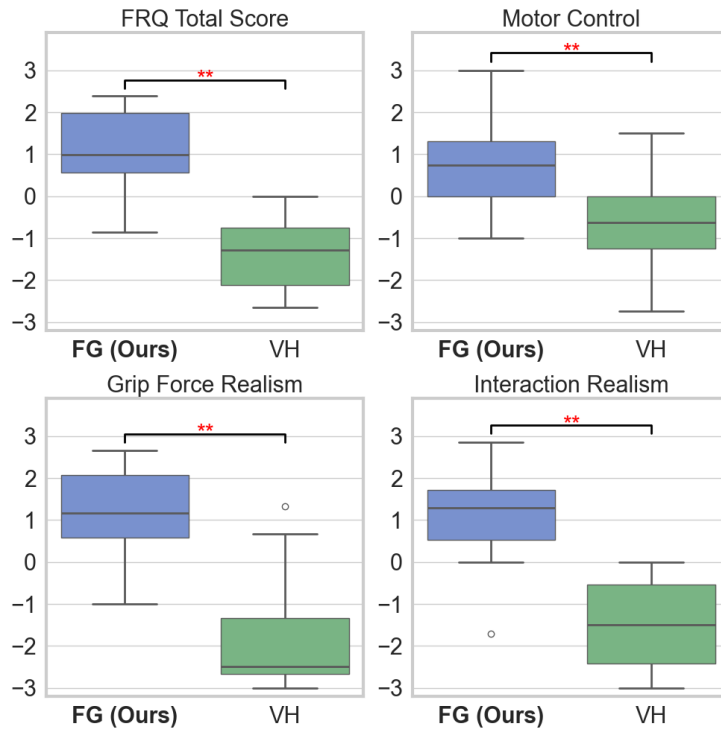


Figure 7: FRQ scores for the Can Squeeze task, using a 7-point Likert scale ranging from -3 (strongly disagree) to +3 (strongly agree). Brackets indicate statistical significances (\* :  $p < .05$ , \*\* :  $p < .01$ ).

As shown in Figure 7, there exist significant differences between FG and VH across all metrics. Detailed statistical comparison results are provided in the supplementary materials. There was no statistically significant change in SSQ scores before and after the experiment.

For FG, many participants reported that “*finely adjusting the force with the trigger*” felt highly intuitive, suggesting faithful translation of user input to grip force. Nonetheless, several noted “*controlling force with a single index trigger felt unnatural*” (P0, P1, P4, P5, P12) and “*the lack of haptic feedback makes fine control more challenging*” (P3, P10, P11, P13). Such issues reflect the broader hardware limitations of consumer VR controllers rather than the ForceGrip itself.

For VH, none of the participants provided positive remarks on force control. Instead, they consistently criticized the “*excessively high grip force regardless of small trigger inputs*” (P1, P2, P3, P4, P5, P6, P8, P15, P19, P20) and described “*difficult or impossible fine-force adjustments*” (P7, P11, P13, P16). These reports align with quantitative findings that the method lacks a reliable mechanism to scale force in response to varying user inputs.

To visualize how closely each system reflects user intentions, we plotted the trigger input against the measured grip force (Figure 8). FG exhibited a clear linear correlation ( $r = 0.884$ ). In contrast, VH showed negligible correlation ( $r = 0.073$ ), consistently producing excessive grip forces irrespective of trigger amplitude. This result contradicts the 1.2 kgf maximum force claimed by Han et al. [2023] and supports reports that VH appears to lack grip force control.

## 7 Conclusion and Future Improvements

We have introduced *ForceGrip*, a novel approach for delivering realistic hand manipulation in VR controller interfaces through faithful grip force control. Unlike many prior systems that rely on narrowly scoped reference datasets, ForceGrip leverages automatically generated training scenarios, thereby improving adaptability and avoiding biases intrinsic to motion-capture data. Our curriculum learning framework further addresses the challenges posed by complex, dynamic interactions, enabling robust convergence and state-of-the-art performance across diverse virtual manipulation tasks.

One significant limitation stems from using standard VR controllers, whose trigger buttons lack fine-grained control and haptic feedback. Future work may explore advanced sensors—such as electromyography,

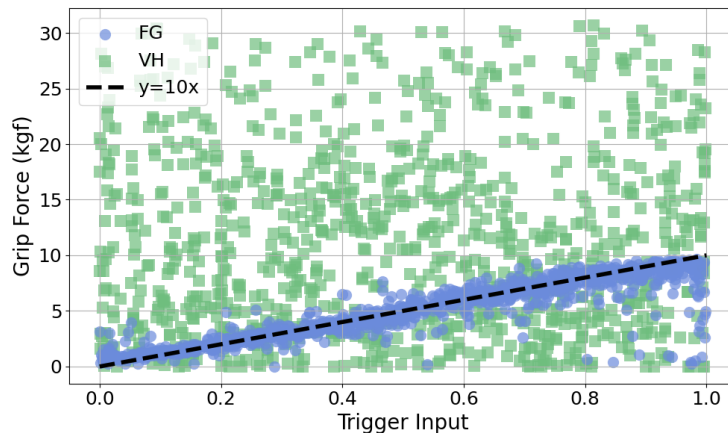


Figure 8: Correlation between trigger input ( $x$ ) and grip force ( $y$ ) for FG and VH, with the reference line ( $y = 10x$ ). Outliers (top 5%) were excluded, and the remaining data was duplicated and resampled to 1,000 points, ensuring an even distribution of trigger values. For FG, points below the reference line mostly occurred when the object slipped from the agent’s grasp.

elastic potentiometers, or pressure sensors—augmented by force-feedback mechanisms to offer richer feedback loops and more intuitive control. Beyond hardware enhancements, improving collision and friction modeling through soft-body simulations could produce more stable and lifelike contact dynamics, particularly for heavier or deformable objects.

## References

- OpenAI: Marcin Andrychowicz, Bowen Baker, Maciek Chociej, Rafal Jozefowicz, Bob McGrew, Jakub Pachocki, Arthur Petron, Matthias Plappert, Glenn Powell, Alex Ray, et al. Learning dexterous in-hand manipulation. *The International Journal of Robotics Research*, 39(1):3–20, 2020.
- Bowen Baker, Ingmar Kanitscheider, Todor Markov, Yi Wu, Glenn Powell, Bob McGrew, and Igor Mordatch. Emergent tool use from multi-agent autotutorials. *arXiv preprint arXiv:1909.07528*, 2019.
- Yoshua Bengio, Jérôme Louradour, Ronan Collobert, and Jason Weston. Curriculum learning. In *Proceedings of the 26th annual international conference on machine learning*, pages 41–48, 2009.
- Kevin Bergamin, Simon Clavet, Daniel Holden, and James Richard Forbes. Drecon: data-driven responsive control of physics-based characters. *ACM Transactions On Graphics (TOG)*, 38(6):1–11, 2019.
- Sammy Christen, Muhammed Kocabas, Emre Aksan, Jemin Hwangbo, Jie Song, and Otmar Hilliges. D-grasp: Physically plausible dynamic grasp synthesis for hand-object interactions. In *Proceedings of the IEEE/CVF Conference on Computer Vision and Pattern Recognition*, pages 20577–20586, 2022.
- Karl Cobbe, Oleg Klimov, Chris Hesse, Taehoon Kim, and John Schulman. Quantifying generalization in reinforcement learning. In *International conference on machine learning*, pages 1282–1289. PMLR, 2019.
- Erwin Coumans and Yunfei Bai. Pybullet, a python module for physics simulation for games, robotics and machine learning, 2016.
- Jieming Cui, Tengyu Liu, Nian Liu, Yaodong Yang, Yixin Zhu, and Siyuan Huang. Anyskill: Learning open-vocabulary physical skill for interactive agents. In *Proceedings of the IEEE/CVF Conference on Computer Vision and Pattern Recognition*, pages 852–862, 2024.
- Carlos Florensa, David Held, Xinyang Geng, and Pieter Abbeel. Automatic goal generation for reinforcement learning agents. In *International conference on machine learning*, pages 1515–1528. PMLR, 2018.
- C Daniel Freeman, Erik Frey, Anton Raichuk, Sertan Girgin, Igor Mordatch, and Olivier Bachem. Brax—a differentiable physics engine for large scale rigid body simulation. *arXiv preprint arXiv:2106.13281*, 2021.
- Mar Gonzalez-Franco and Tabitha C Peck. Avatar embodiment. towards a standardized questionnaire. *Frontiers in Robotics and AI*, 5:74, 2018.

- Alex Graves, Marc G Bellemare, Jacob Menick, Remi Munos, and Koray Kavukcuoglu. Automated curriculum learning for neural networks. In *international conference on machine learning*, pages 1311–1320. Pmlr, 2017.
- Tuomas Haarnoja, Ben Moran, Guy Lever, Sandy H Huang, Dhruva Tirumala, Jan Humplik, Markus Wulfmeier, Saran Tunyasuvunakool, Noah Y Siegel, Roland Hafner, et al. Learning agile soccer skills for a bipedal robot with deep reinforcement learning. *Science Robotics*, 9(89):eadi8022, 2024.
- Guy Hachohen and Daphna Weinshall. On the power of curriculum learning in training deep networks. In *International conference on machine learning*, pages 2535–2544. PMLR, 2019.
- DongHeun Han, RoUn Lee, KyeongMin Kim, and HyeongYeop Kang. Vr-handnet: A visually and physically plausible hand manipulation system in virtual reality. *IEEE Transactions on Visualization and Computer Graphics*, 2023.
- Mohamed Hassan, Yunrong Guo, Tingwu Wang, Michael Black, Sanja Fidler, and Xue Bin Peng. Synthesizing physical character-scene interactions. In *ACM SIGGRAPH 2023 Conference Proceedings*, pages 1–9, 2023.
- Nicolas Heess, Dhruva Tb, Srinivasan Sriram, Jay Lemmon, Josh Merel, Greg Wayne, Yuval Tassa, Tom Erez, Ziyu Wang, SM Eslami, et al. Emergence of locomotion behaviours in rich environments. *arXiv preprint arXiv:1707.02286*, 2017.
- Dan Hendrycks and Kevin Gimpel. Gaussian error linear units (gelus). *arXiv preprint arXiv:1606.08415*, 2016.
- Jonathan Ho and Stefano Ermon. Generative adversarial imitation learning. *Advances in neural information processing systems*, 29, 2016.
- Markus Höll, Markus Oberweger, Clemens Arth, and Vincent Lepetit. Efficient physics-based implementation for realistic hand-object interaction in virtual reality. In *2018 IEEE conference on virtual reality and 3D user interfaces (VR)*, pages 175–182. IEEE, 2018.
- Yuanming Hu, Luke Anderson, Tzu-Mao Li, Qi Sun, Nathan Carr, Jonathan Ragan-Kelley, and Frédo Durand. DiffTaichi: Differentiable programming for physical simulation. *arXiv preprint arXiv:1910.00935*, 2019.
- Jordan Juravsky, Yunrong Guo, Sanja Fidler, and Xue Bin Peng. Padl: Language-directed physics-based character control. In *SIGGRAPH Asia 2022 Conference Papers*, pages 1–9, 2022.
- Niels Justesen, Ruben Rodriguez Torrado, Philip Bontrager, Ahmed Khalifa, Julian Togelius, and Sebastian Risi. Illuminating generalization in deep reinforcement learning through procedural level generation. *arXiv preprint arXiv:1806.10729*, 2018.
- Jari Kangas, Sriram Kishore Kumar, Helena Mehtonen, Jorma Järnstedt, and Roope Raisamo. Trade-off between task accuracy, task completion time and naturalness for direct object manipulation in virtual reality. *Multimodal Technologies and Interaction*, 6(1):6, 2022.
- Robert S Kennedy, Norman E Lane, Kevin S Berbaum, and Michael G Lilienthal. Simulator sickness questionnaire: An enhanced method for quantifying simulator sickness. *The international journal of aviation psychology*, 3(3):203–220, 1993.
- Arnaud Klipfel, Nitish Sontakke, Ren Liu, and Sehoon Ha. Learning a single policy for diverse behaviors on a quadrupedal robot using scalable motion imitation. In *2023 IEEE/RSJ International Conference on Intelligent Robots and Systems (IROS)*, pages 2768–2775. IEEE, 2023.
- Vikash Kumar and Emanuel Todorov. Mujoco haptix: A virtual reality system for hand manipulation. In *2015 IEEE-RAS 15th International Conference on Humanoid Robots (Humanoids)*, pages 657–663. IEEE, 2015.
- Kyungho Lee, Sehee Min, Sunmin Lee, and Jehee Lee. Learning time-critical responses for interactive character control. *ACM Transactions on Graphics (TOG)*, 40(4):1–11, 2021a.
- Seyoung Lee, Sunmin Lee, Yongwoo Lee, and Jehee Lee. Learning a family of motor skills from a single motion clip. *ACM Transactions on Graphics (TOG)*, 40(4):1–13, 2021b.

- Eric Liang, Richard Liaw, Robert Nishihara, Philipp Moritz, Roy Fox, Ken Goldberg, Joseph Gonzalez, Michael Jordan, and Ion Stoica. Rllib: Abstractions for distributed reinforcement learning. In *International conference on machine learning*, pages 3053–3062. PMLR, 2018.
- Siqi Liu, Guy Lever, Zhe Wang, Josh Merel, SM Ali Eslami, Daniel Hennes, Wojciech M Czarnecki, Yuval Tassa, Shayegan Omidshafiei, Abbas Abdolmaleki, et al. From motor control to team play in simulated humanoid football. *Science Robotics*, 7(69):eabo0235, 2022.
- Ying-Sheng Luo, Jonathan Hans Soeseno, Trista Pei-Chun Chen, and Wei-Chao Chen. Carl: Controllable agent with reinforcement learning for quadruped locomotion. *ACM Transactions on Graphics (TOG)*, 39(4):38–1, 2020.
- Zhengyi Luo, Jinkun Cao, Kris Kitani, Weipeng Xu, et al. Perpetual humanoid control for real-time simulated avatars. In *Proceedings of the IEEE/CVF International Conference on Computer Vision*, pages 10895–10904, 2023.
- Viktor Makoviychuk, Lukasz Wawrzyniak, Yunrong Guo, Michelle Lu, Kier Storey, Miles Macklin, David Hoeller, Nikita Rudin, Arthur Allshire, Ankur Handa, et al. Isaac gym: High performance gpu-based physics simulation for robot learning. *arXiv preprint arXiv:2108.10470*, 2021.
- Sanmit Narvekar and Peter Stone. Learning curriculum policies for reinforcement learning. *arXiv preprint arXiv:1812.00285*, 2018.
- Sanmit Narvekar, Bei Peng, Matteo Leonetti, Jivko Sinapov, Matthew E Taylor, and Peter Stone. Curriculum learning for reinforcement learning domains: A framework and survey. *Journal of Machine Learning Research*, 21(181):1–50, 2020.
- Sergiu Oprea, Pablo Martinez-Gonzalez, Alberto Garcia-Garcia, John A Castro-Vargas, Sergio Orts-Escolano, and Jose Garcia-Rodriguez. A visually realistic grasping system for object manipulation and interaction in virtual reality environments. *Computers & Graphics*, 83:77–86, 2019.
- SooHwan Park, Hoseok Ryu, Seyoung Lee, Sunmin Lee, and Jehee Lee. Learning predict-and-simulate policies from unorganized human motion data. *ACM Transactions on Graphics (TOG)*, 38(6):1–11, 2019.
- Xue Bin Peng, Glen Berseth, KangKang Yin, and Michiel Van De Panne. Deeploco: Dynamic locomotion skills using hierarchical deep reinforcement learning. *Acm transactions on graphics (tog)*, 36(4):1–13, 2017.
- Xue Bin Peng, Pieter Abbeel, Sergey Levine, and Michiel Van de Panne. Deepmimic: Example-guided deep reinforcement learning of physics-based character skills. *ACM Transactions On Graphics (TOG)*, 37(4):1–14, 2018.
- Xue Bin Peng, Ze Ma, Pieter Abbeel, Sergey Levine, and Angjoo Kanazawa. Amp: Adversarial motion priors for stylized physics-based character control. *ACM Transactions on Graphics (ToG)*, 40(4):1–20, 2021.
- Xue Bin Peng, Yunrong Guo, Lina Halper, Sergey Levine, and Sanja Fidler. Ase: Large-scale reusable adversarial skill embeddings for physically simulated characters. *ACM Transactions On Graphics (TOG)*, 41(4):1–17, 2022.
- Wei Quan, He Yang, Cheng Han, and Yinong Li. Realistic interaction system for human hand in virtual environments. In *2020 International Conference on Intelligent Transportation, Big Data & Smart City (ICITBS)*, pages 772–778. IEEE, 2020.
- Aravind Rajeswaran, Vikash Kumar, Abhishek Gupta, Giulia Vezzani, John Schulman, Emanuel Todorov, and Sergey Levine. Learning complex dexterous manipulation with deep reinforcement learning and demonstrations. *arXiv preprint arXiv:1709.10087*, 2017.
- John Schulman, Filip Wolski, Prafulla Dhariwal, Alec Radford, and Oleg Klimov. Proximal policy optimization algorithms. *arXiv preprint arXiv:1707.06347*, 2017.
- Yinghan Shi, Lizhi Zhao, Xuequan Lu, Thuong Hoang, and Meili Wang. Grasping 3d objects with virtual hand in vr environment. In *Proceedings of the 18th ACM SIGGRAPH International Conference on Virtual-Reality Continuum and its Applications in Industry*, pages 1–8, 2022.

- Felipe Leno Da Silva and Anna Helena Reali Costa. Object-oriented curriculum generation for reinforcement learning. In *Proceedings of the 17th international conference on autonomous agents and multiagent systems*, pages 1026–1034, 2018.
- Richard S Sutton and Andrew G Barto. Reinforcement learning: An introduction. *Robotica*, 17(2):229–235, 1999.
- Jie Tan, Karen Liu, and Greg Turk. Stable proportional-derivative controllers. *IEEE Computer Graphics and Applications*, 31(4):34–44, 2011.
- Emanuel Todorov, Tom Erez, and Yuval Tassa. Mujoco: A physics engine for model-based control. In *2012 IEEE/RSJ international conference on intelligent robots and systems*, pages 5026–5033. IEEE, 2012.
- Eros Viola, Fabio Solari, and Manuela Chessa. Small objects manipulation in immersive virtual reality. In *VISIGRAPP (2: HUCAPP)*, pages 233–240, 2022.
- Jan-Niklas Voigt-Antons, Tanja Kojic, Danish Ali, and Sebastian Möller. Influence of hand tracking as a way of interaction in virtual reality on user experience. In *2020 Twelfth International Conference on Quality of Multimedia Experience (QoMEX)*, pages 1–4. IEEE, 2020.
- Rui Wang, Joel Lehman, Jeff Clune, and Kenneth O Stanley. Paired open-ended trailblazer (poet): Endlessly generating increasingly complex and diverse learning environments and their solutions. *arXiv preprint arXiv:1901.01753*, 2019.
- Tingwu Wang, Yunrong Guo, Maria Shugrina, and Sanja Fidler. Unicon: Universal neural controller for physics-based character motion. *arXiv preprint arXiv:2011.15119*, 2020.
- Daphna Weinshall, Gad Cohen, and Dan Amir. Curriculum learning by transfer learning: Theory and experiments with deep networks. In *International conference on machine learning*, pages 5238–5246. PMLR, 2018.
- Jungdam Won and Jehhee Lee. Learning body shape variation in physics-based characters. *ACM Transactions on Graphics (TOG)*, 38(6):1–12, 2019.
- Jungdam Won, Deepak Gopinath, and Jessica Hodgins. Control strategies for physically simulated characters performing two-player competitive sports. *ACM Transactions on Graphics (TOG)*, 40(4):1–11, 2021.
- Jungdam Won, Deepak Gopinath, and Jessica Hodgins. Physics-based character controllers using conditional vaes. *ACM Transactions on Graphics (TOG)*, 41(4):1–12, 2022.
- Zeshi Yang, Kangkang Yin, and Libin Liu. Learning to use chopsticks in diverse gripping styles. *ACM Transactions on Graphics (TOG)*, 41(4):1–17, 2022.
- He Zhang, Yuting Ye, Takaaki Shiratori, and Taku Komura. Manipnet: neural manipulation synthesis with a hand-object spatial representation. *ACM Transactions on Graphics (ToG)*, 40(4):1–14, 2021.
- Hui Zhang, Sammy Christen, Zicong Fan, Luocheng Zheng, Jemin Hwangbo, Jie Song, and Otmar Hilliges. Artigrasp: Physically plausible synthesis of bi-manual dexterous grasping and articulation. In *2024 International Conference on 3D Vision (3DV)*, pages 235–246. IEEE, 2024.

## A PPO hyperparameters

The parameters for proximal policy optimization (PPO) are shown in Table 3.

Table 3: PPO hyperparameters used in the experiment

Parameter	Value	Parameter	Value
Actor learning rate	0.0001	PPO epochs	16
Critic learning rate	0.001	Episode batch size	3000
Discount factor	0.98	Mini batch size	3000
GAE parameter	0.95		
Clipping parameter ( $\epsilon$ )	0.2		
Entropy coefficient	0.01		

## B Detailed Network Architecture

Detailed network architecture is illustrated in Figure 9.

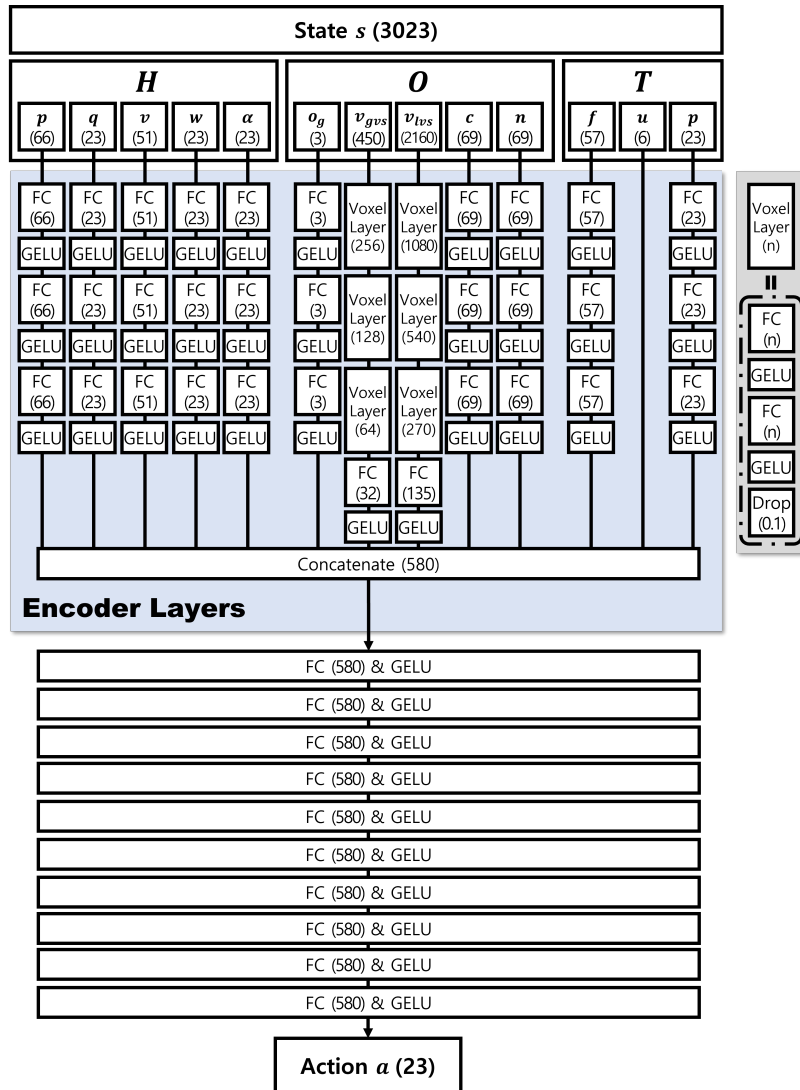


Figure 9: Detailed network architecture. FC(nn) represents a fully connected layer with n nodes, and Drop(0.1) denotes a dropout layer with a rate of 0.1.



## C Trigger flow generation

The algorithms used for various trigger flow generation are described in algorithm 1.

---

### Algorithm 1: Generate Noisy Trigger Flow

---

**Input:** Time Range  $t_0$  to  $t_T$ , Frequency Range  $[f_{\min}, f_{\max}]$ , Amplitude Range  $[A_{\min}, A_{\max}]$ , Offset Range  $[O_{\min}, O_{\max}]$ , Noise Parameters  $\sigma$  (std. deviation), clip (max noise magnitude)

**Output:** Noisy trigger sequence  $\{u_t\}_{t=t_0}^{t_T}$

**Step 1: Generate Random Parameters;**

$f \leftarrow \text{RandomUniform}(f_{\min}, f_{\max})$  ;

/\* Frequency \*/

$A \leftarrow \text{RandomUniform}(A_{\min}, A_{\max})$  ;

/\* Amplitude \*/

$O \leftarrow \text{RandomUniform}(O_{\min}, O_{\max})$  ;

/\* Offset \*/

$\phi \leftarrow \text{RandomUniform}(0, 2\pi)$  ;

/\* Initial Phase \*/

**Step 2: Compute Trigger for Each  $t$ ;**

**for**  $t \leftarrow t_0$  **to**  $t_T$  **do**

$\text{sin\_trigger} \leftarrow A \cdot \sin(2\pi ft + \phi) + 0.5 + O$ ;

$\text{noise} \leftarrow \text{Clamp}(\sigma \cdot \text{RandomGaussian}(), -\text{clip}, \text{clip})$ ;

$\text{trigger}_t \leftarrow \text{Clamp01}(\text{sin\_trigger} + \text{noise})$ ;

**end**

**return**  $\{\text{trigger}_t\}_{t=t_0}^{t_T}$ ;

---

The parameters for noisy trigger flow generation are shown in Table 4.

Table 4: Parameters for Noisy Trigger Flow Generation

Description / Range	Value
Frequency range ( $[f_{\min}, f_{\max}]$ )	[0.833, 0.5]
Amplitude range ( $[A_{\min}, A_{\max}]$ )	[0.0, 2.0]
Offset range ( $[O_{\min}, O_{\max}]$ )	[-1.0, 1.0]
Noise standard deviation ( $\sigma$ )	0.05
Maximum noise magnitude (clip)	0.1

The examples of the generated trigger flow can be found in Figure 10.

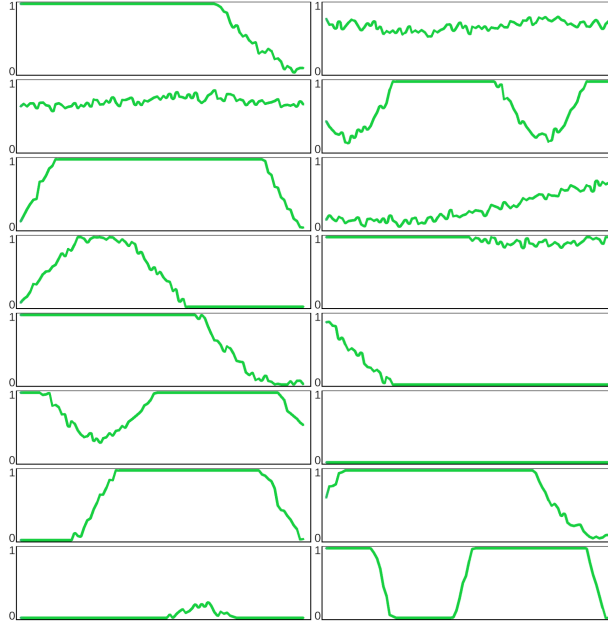


Figure 10: Generated trigger flow examples illustrate the diverse dynamics of noisy synthetic inputs, combining sinusoidal components and Gaussian noise. Each plot represents flow patterns over time (3 s), showcasing behaviors such as gradual activation, periodic oscillations, transient bursts, and steady states, reflecting the natural variability of user behavior.

## D Force Realism Questionnaire

The list of questions in the Force Realism Questionnaire (FRQ) is shown in Table 5. Each item was evaluated using a 7-point Likert scale anchored at "strongly disagree (-3)" and "strongly agree (+3)."

Table 5: Force realism questionnaire

ID	Question
<b>Aspect 1: Motor Control</b>	
Q1.	I felt like I could control the grip force as if it were my own hand's grip force
Q2.	The adjustment of the grip force was caused by my controls
Q3.	I felt as if the grip force of the virtual hand was influencing my own control
Q4.	I felt as if the virtual hand applied grip force by itself
<b>Aspect 2: Grip Force Realism</b>	
Q5.	It seemed that the grip force change was smooth and plausible
Q6.	I felt the grip force was applied and released in a natural way
Q7.	Grip forces reacted adequately to my intentions
<b>Aspect 3: Interaction Realism</b>	
Q8.	I felt like I could adjust the grip force to the object wherever I wanted to
Q9.	It seemed as if the virtual fingers were mine when applying grip forces to an object
Q10.	I felt that adjusting the grip force was clumsy and hard to achieve
Q11.	It seemed as if the grip force was guided and unnatural
Q12.	I felt that the grip force was visually correct and natural
Q13.	I felt that the grip force was physically correct and natural
Q14.	It seemed that the grip force was adapting properly to different geometries

The FRQ consists of three categories, calculated as follows:

$$\text{Motor Control (MC)} = ((Q1 + Q2) - (Q3 + Q4)) / 4 \quad (5)$$

$$\text{Grip Force Realism (GFR)} = (Q5 + Q6 + Q7) / 3 \quad (6)$$

$$\text{Interaction Realism (IR)} = ((Q8 + Q9) - (Q10 + Q11) + Q12 + Q13 + Q14) / 7 \quad (7)$$

$$\text{FCQ Score} = (\text{MC} + \text{FMR} + \text{IR} * 2) / 4 \quad (8)$$

The scoring methodology for the FRQ was adapted from the realism questionnaire (RQ) in Oprea et al. [2019], with the same calculations applied to the RQ's items as well.

## E Detailed statistical comparison results

### E.1 E1: Pick-and-place result

For the pick-and-place experiment, three methods were evaluated: *ForceGrip* (FG), *Attachment* (AT) Oprea et al. [2019] and *VR-HandNet* (VH) Han et al. [2023].

For the RQ total score, FG scored  $1.417 \pm 0.862$ , VH scored  $-0.206 \pm 1.497$ , and AT scored  $0.460 \pm 1.050$ . A Friedman test revealed a highly significant difference ( $p$ -value = 0.0002,  $p < 0.01$ ). For the RQ motor control score, FG had a score of  $1.300 \pm 1.002$ , VH scored  $0.325 \pm 1.428$ , and AT scored  $0.588 \pm 0.792$ , with the Friedman test showing a significant difference ( $p$ -value = 0.0080,  $p < 0.01$ ). Regarding the RQ finger movement realism score, FG scored  $1.567 \pm 1.170$ , VH scored  $-0.433 \pm 1.758$ , and AT scored  $0.467 \pm 1.322$ , with a highly significant difference indicated by a Friedman test ( $p$ -value = 0.0001,  $p < 0.01$ ). For the RQ interaction realism score, FG scored  $1.400 \pm 1.024$ , VH scored  $-0.357 \pm 1.691$ , and AT scored  $0.393 \pm 1.268$ , with the Friedman test also showing a highly significant difference ( $p$ -value = 0.0001,  $p < 0.01$ ).

Pairwise comparisons revealed that for the total score, FG scored significantly higher than VH ( $p = 0.0001$ ,  $p < 0.01$ ) and AT ( $p = 0.0027$ ,  $p < 0.01$ ), while the difference between VH and AT was not significant ( $p = 0.1650$ ). For the motor control score, FG scored significantly higher than VH ( $p = 0.0077$ ,  $p < 0.01$ ) and AT ( $p = 0.0216$ ,  $p < 0.05$ ), while the difference between VH and AT was not significant ( $p = 0.8955$ ). In the finger movement realism score, FG was significantly higher than VH ( $p = 0.0006$ ,  $p < 0.01$ ) and AT ( $p = 0.0017$ ,  $p < 0.01$ ), with no significant difference between VH and AT ( $p = 0.0625$ ). Finally, for the interaction realism score, FG scored significantly higher than VH ( $p = 0.0004$ ,  $p < 0.01$ ) and AT ( $p = 0.0032$ ,  $p < 0.01$ ), while VH and AT did not differ significantly ( $p = 0.0897$ ).

## E.2 E2: Can squeeze result

For the can-squeeze experiment, two methods were evaluated: *ForceGrip* (FG) and *VR-HandNet* (VH) Han et al. [2023].

For the FRQ total score, FG scored  $1.124 \pm 0.838$ , while VH scored  $-1.357 \pm 0.816$ , with a highly significant difference ( $p$ -value = 0.0000,  $p < 0.01$ ). Regarding the FRQ motor control score, FG achieved  $0.900 \pm 1.032$  compared to VH's  $-0.613 \pm 1.014$  ( $p$ -value = 0.0002,  $p < 0.01$ ). For the FRQ grip force realism score, FG scored  $1.267 \pm 0.981$ , surpassing VH's  $-1.900 \pm 1.221$  ( $p$ -value = 0.0001,  $p < 0.01$ ). Similarly, for the FRQ interaction realism score, FG's  $1.164 \pm 1.023$  outperformed VH's  $-1.457 \pm 0.941$ , demonstrating a highly significant difference ( $p$ -value = 0.0000,  $p < 0.01$ ).